Supporting Information

Porosity Meets Robustness: Design of Ultralight MXene/PVA Composite Foams for High-Performance Flexible Supercapacitors

Zifang Zhao, Zhilong Xu, Weifeng Huang, Jingteng Feng, Guangri Xu, Yuanchao Li, Yalei Wang,* Qichong Zhang* and Wai-Yeung Wong*

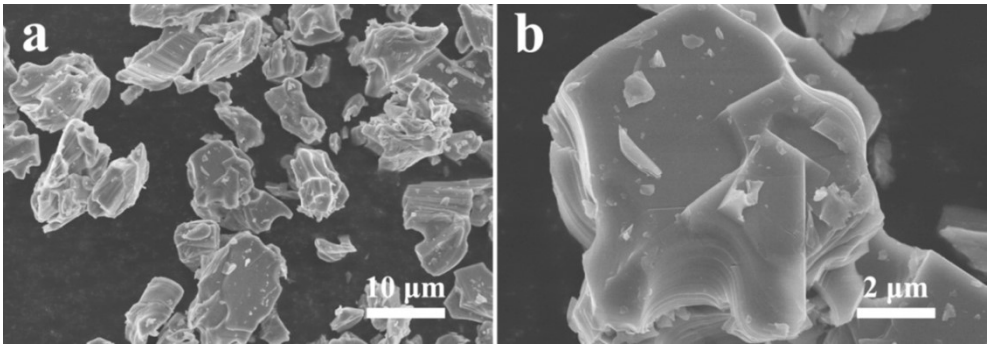

Fig. S1 SEM images of Ti_3AlC_2 particles.

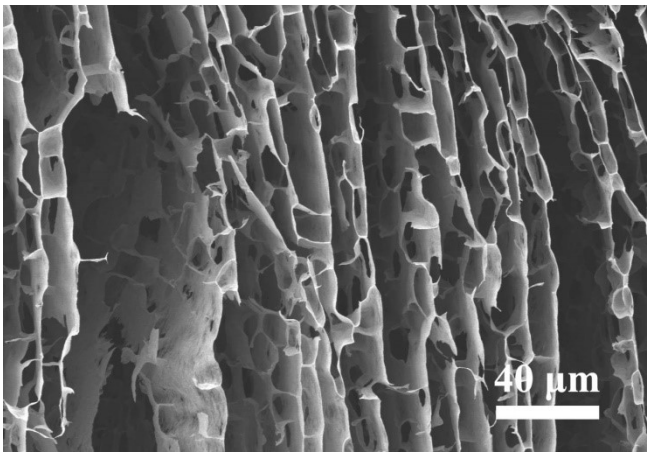

Fig. S2 SEM images of freeze-dried $Ti_3C_2T_x$ MXene.

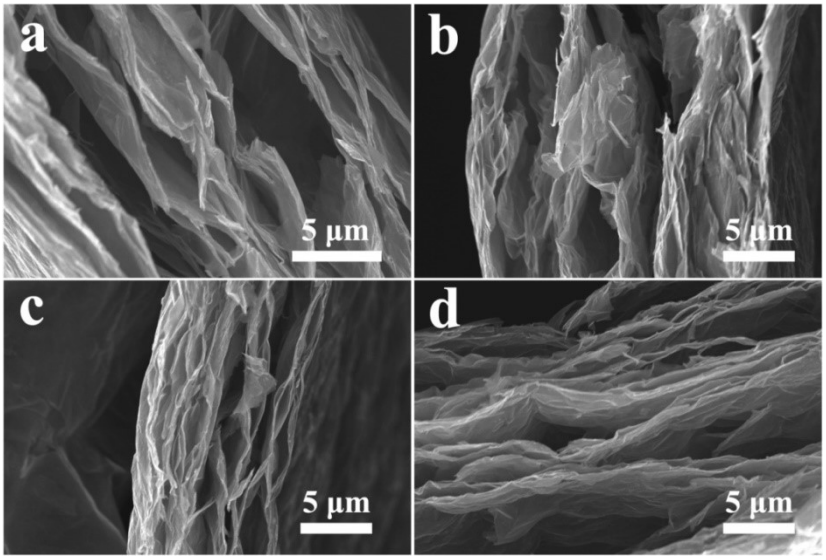

Fig. S3 SEM images of MH1-20: a) MH1, b) MH5, c) MH10 and d) MH20.

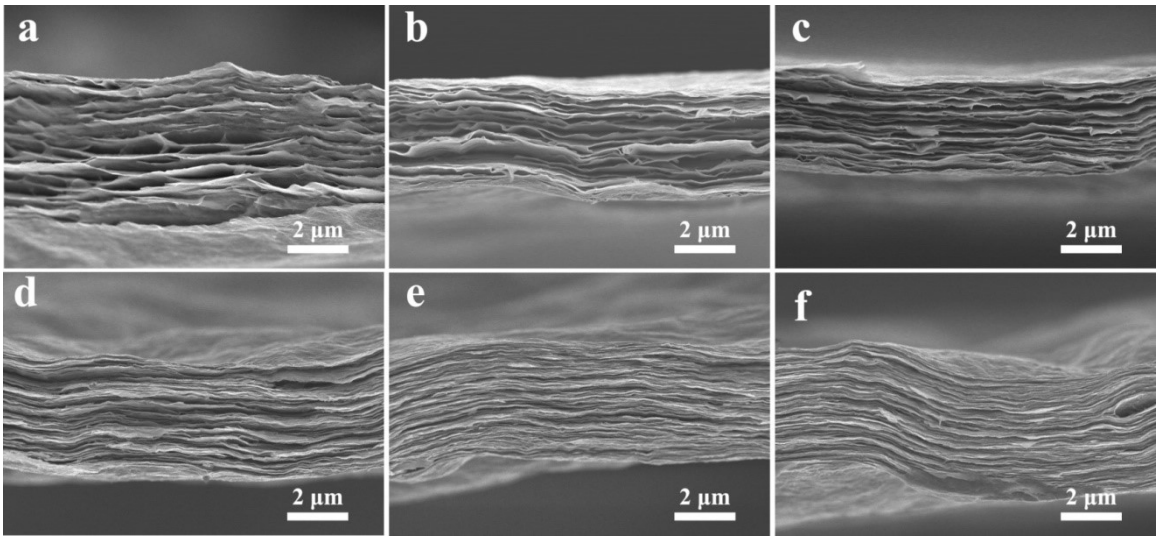

Fig. S4 SEM images of MP1-20: a) MP1, b) MP5, c) MP10, d) MP15, and e) MP20.

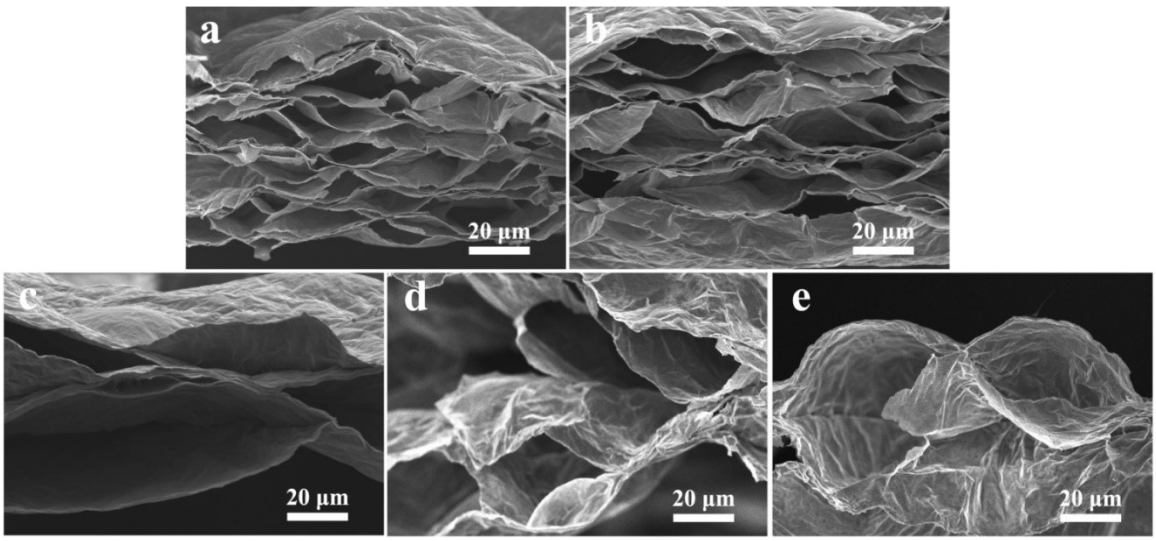

Fig. S5 SEM images of MPH1-20: a) MPH1, b) MPH5, c) MPH10, d) MPH15, and e) MPH20.

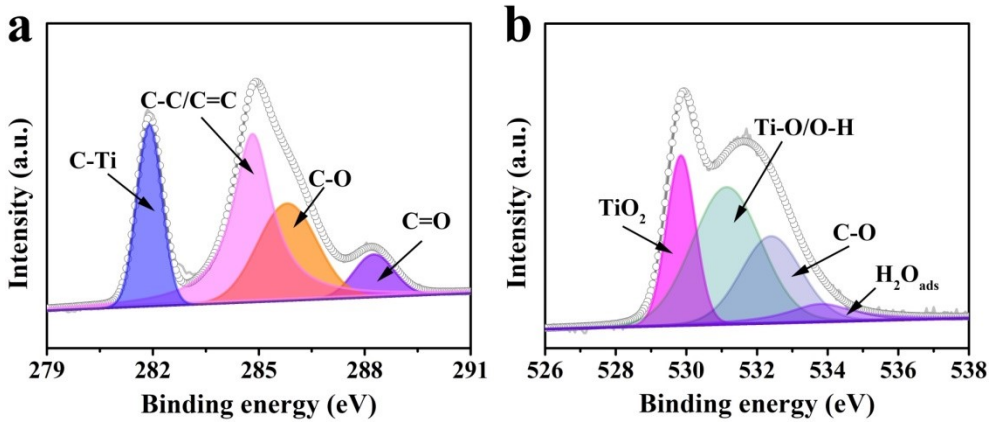

Fig. S6 XPS a) C 1s and b) O 1s spectra of MXene films treated with H_2O.

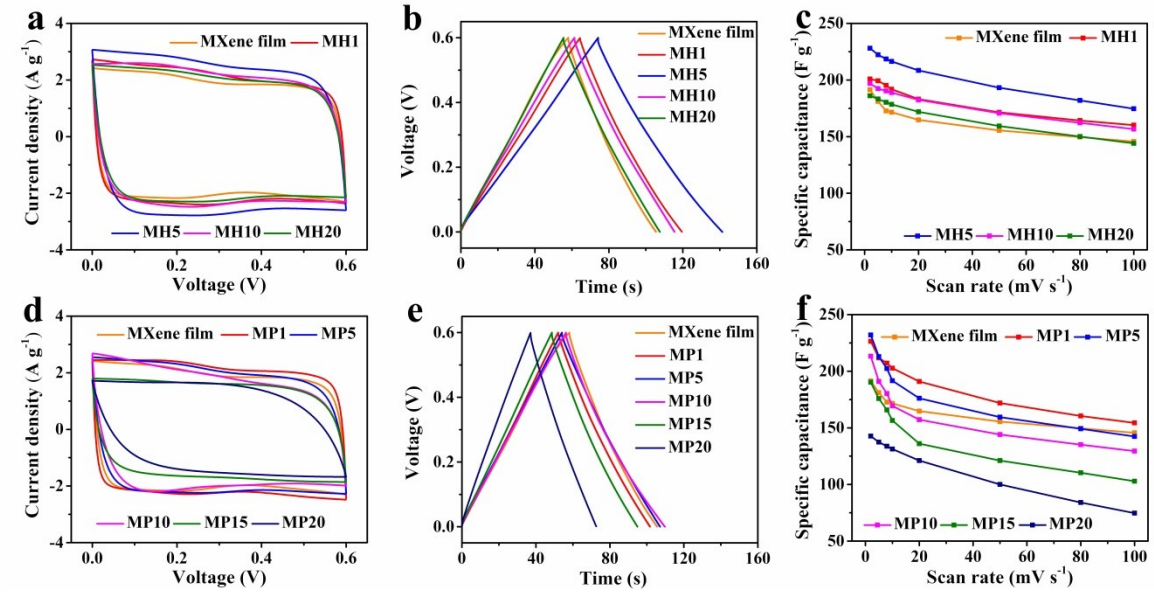

Fig. S7 Electrochemical performance of MXene films, MH1-20, and MP1-20: a,d) CV curves at the scan rate of 50 mV s^{-1}; b,e) GCD plots with a current density of 0.5 A g^{-1}; c,f) specific capacitance under different scan rates.

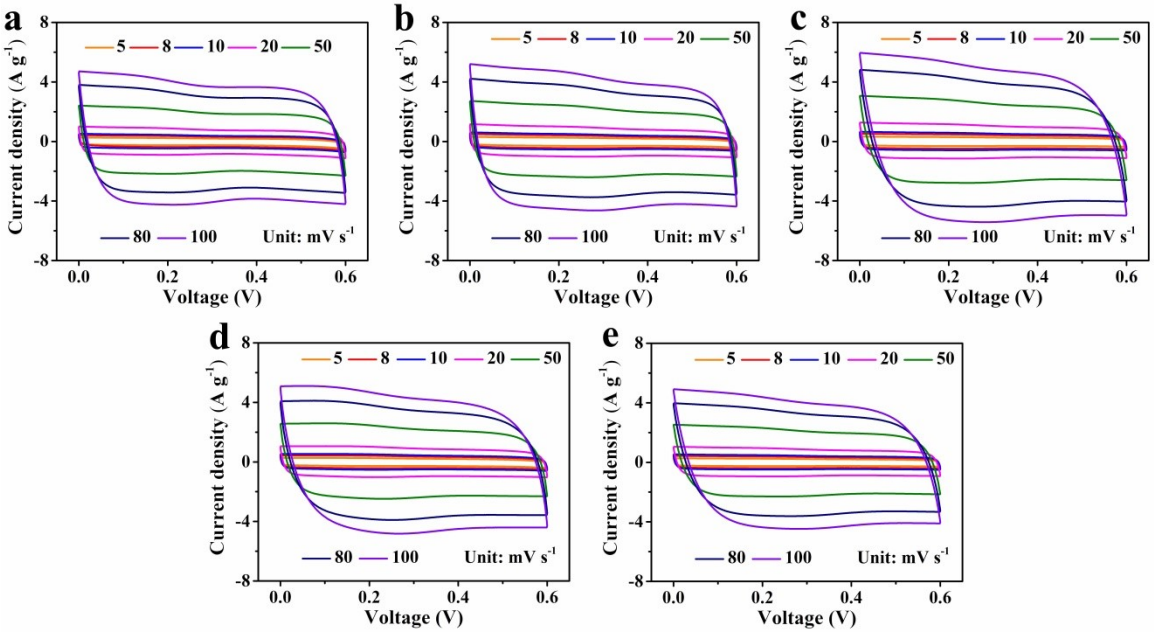

Fig. S8 CV curves of a) MXene films and MH1-20: b) MH1, c) MH5, d) MH10 and e) MH20.

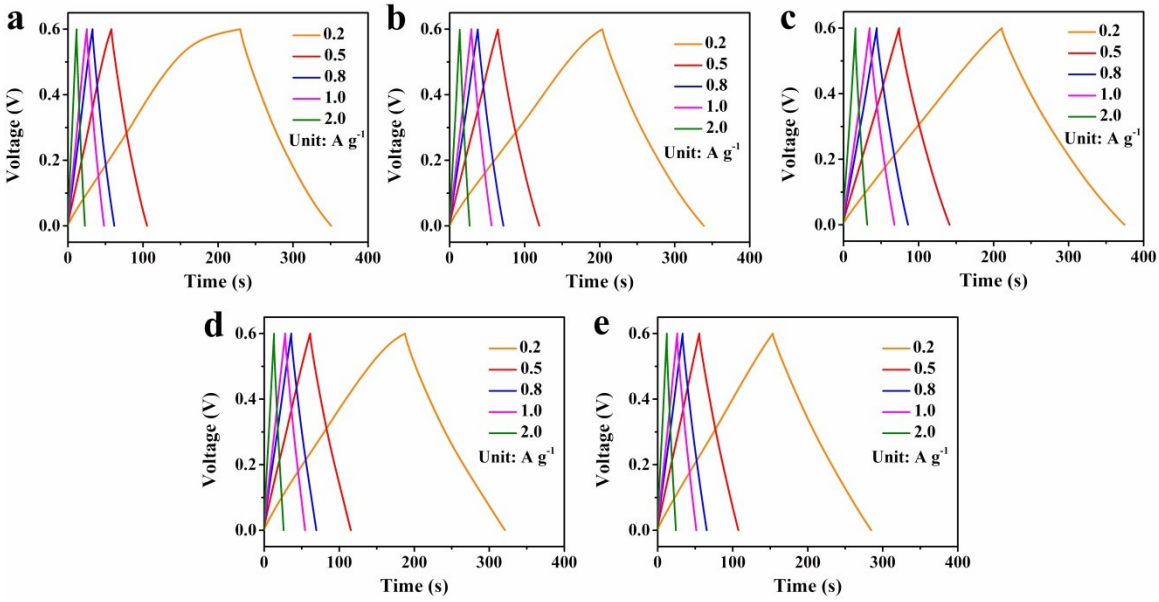

Fig. S9 GCD curves of a) MXene films and MH1-20: b) MH1, c) MH5, d) MH10 and e) MH20.

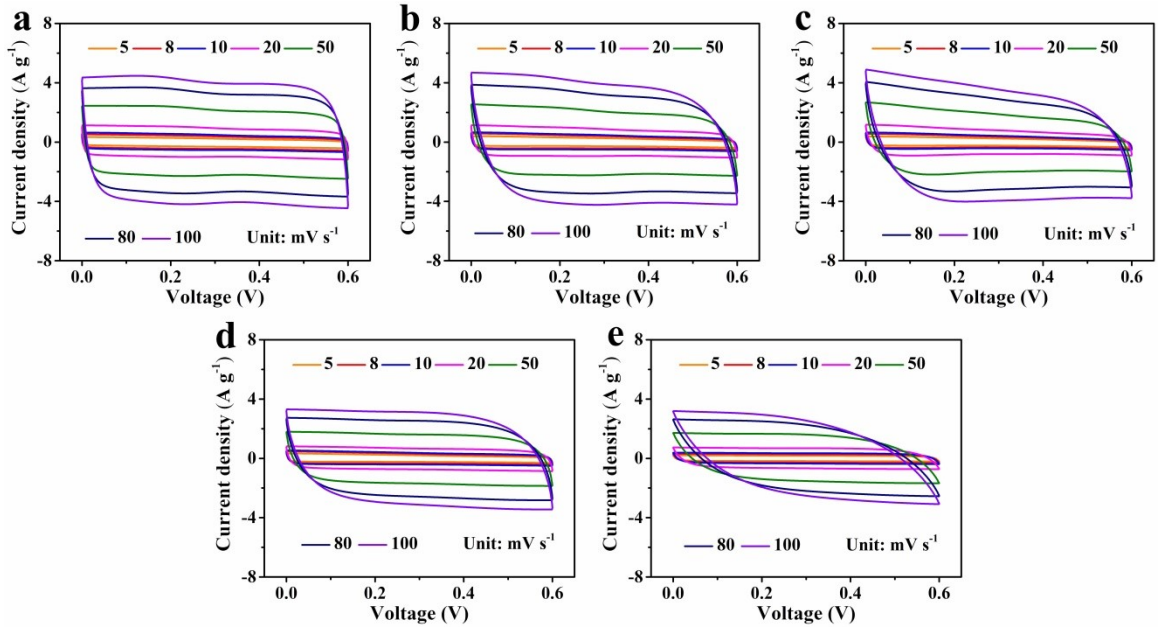

Fig. S10 CV curves of MP1-20: a) MP1, b) MP5, c) MP10, d) MP15, and e) MP20.

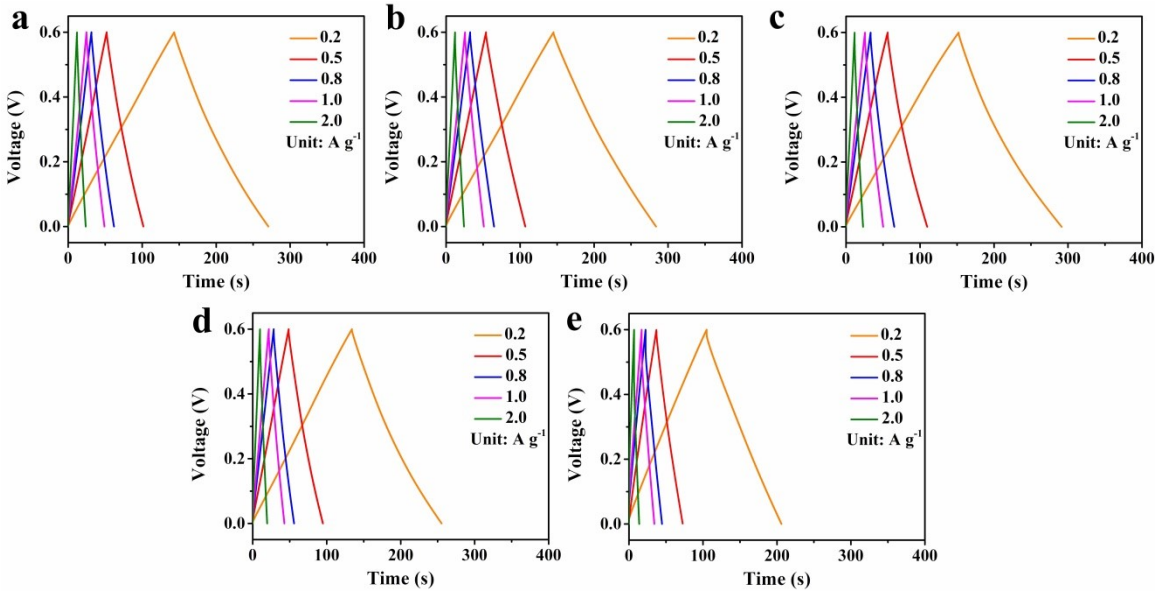

Fig. S11 GCD curves of MP1-20: a) MP1, b) MP5, c) MP10, d) MP15, and e) MP20.

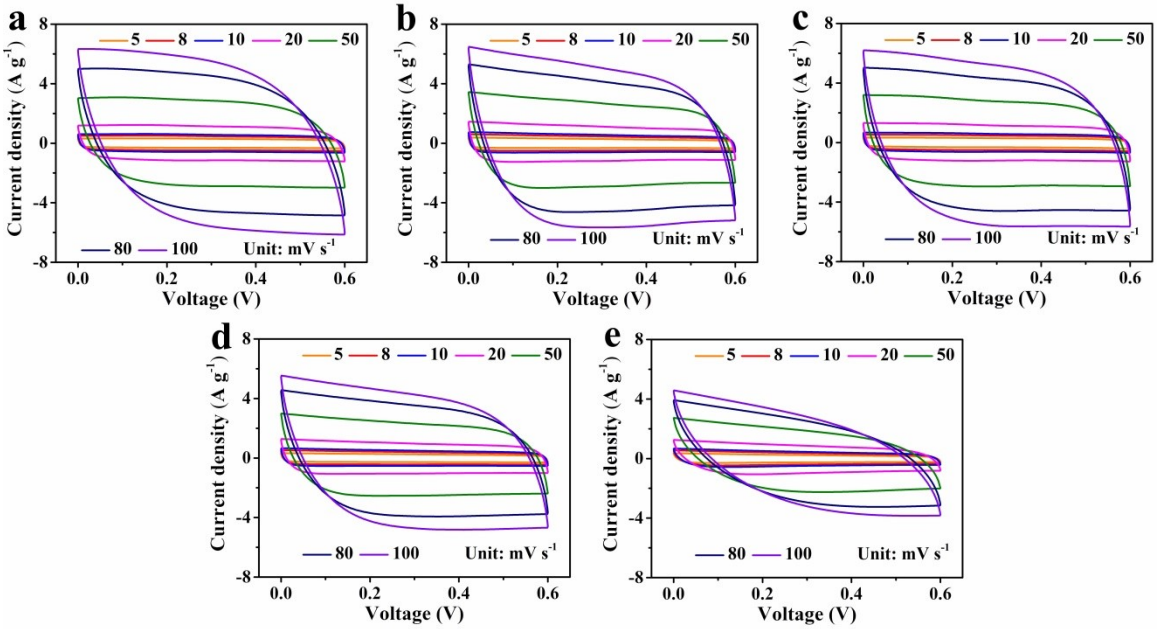

Fig. S12 CV curves of MPH1-20: a) MPH1, b) MPH5, c) MPH10, d) MPH15, and e) MPH20.

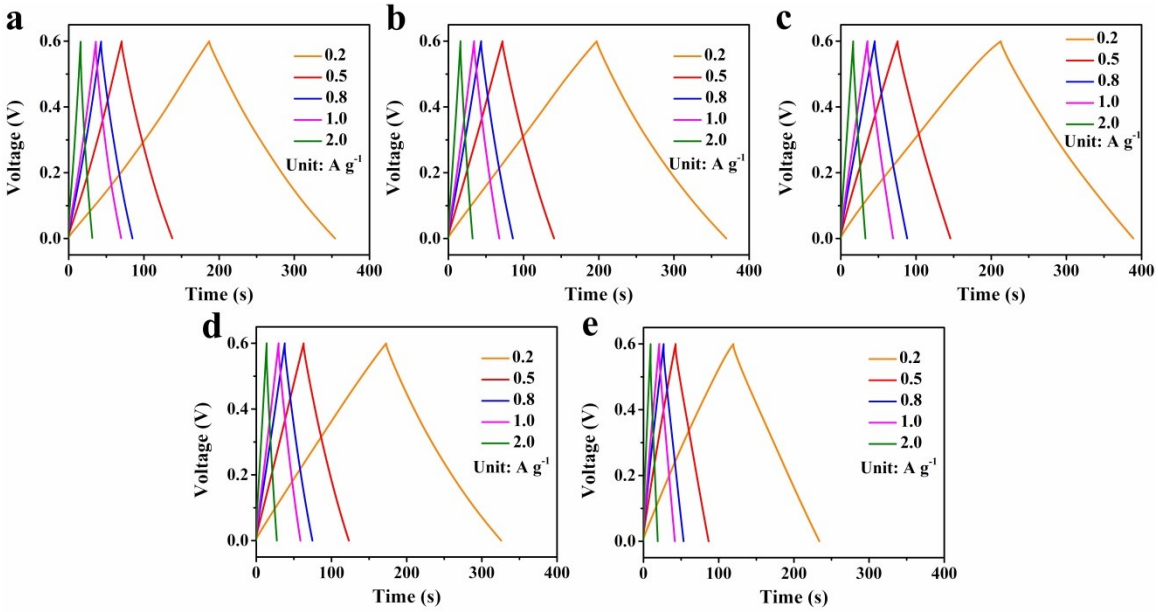

Fig. S13 GCD curves of MPH1-20: a) MPH1, b) MPH5, c) MPH10, d) MPH15, and e) MPH20.

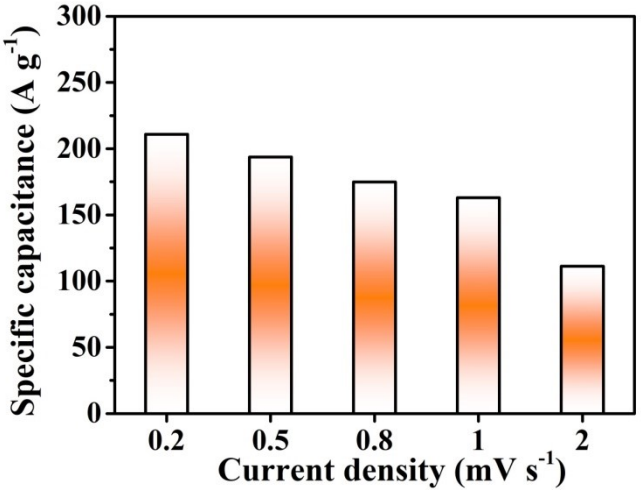

Fig. S14 Specific capacitances of the flexible supercapacitor depend on current density.

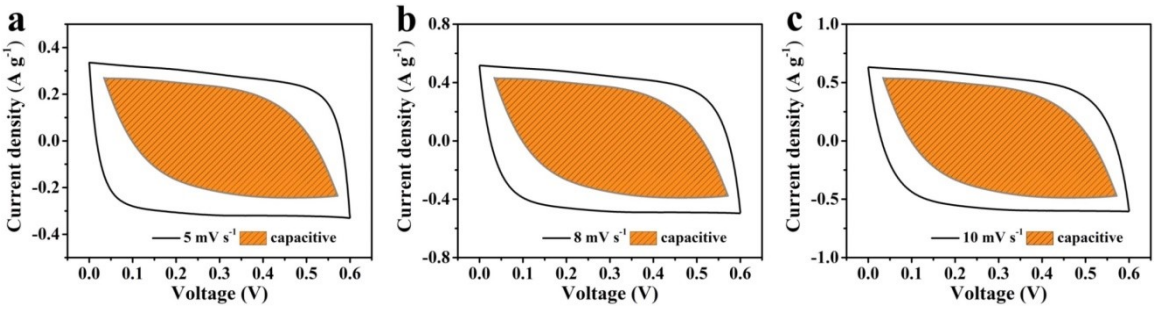

Fig. S15 CV curves of the flexible supercapacitor with a capacitance contribution at a) 5, b) 8, and c) 10 mV s^{-1}, respectively.